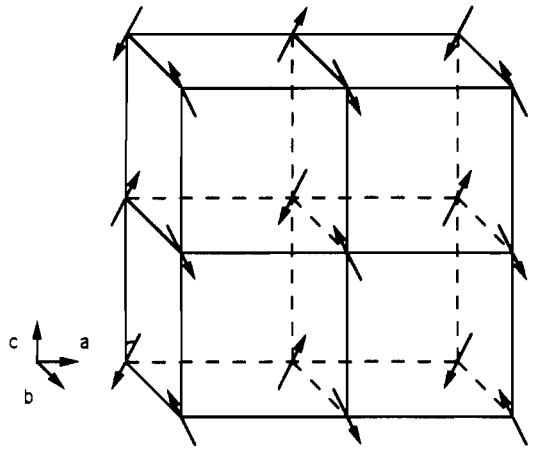

Figure 8. Possible spin configuration for 2[4-halopyridinium tetrachloroferrate(III)]-4-halopyridinium halide. The canting angle is greatly exaggerated in the drawing.

and where z is the number of nearest neighbors and S is the spin.

To avoid the usual poor prediction of the transition temperature by molecular field theory (MFT), T_c may be set to the actual transition temperature. In that case

$$\chi_{\perp}^{\text{cant}} = \chi_c \frac{T - T_c/[1 + (D/2J)^2]^{0.5}}{T^2 - T_c^2} \qquad (7)$$

A preliminary fit of this equation to 2[4-Cl(py)H][$FeCl_4$]·[4-Cl(py)H]Cl data along the canting direction was not good, partly because the data rise faster and sharper than the simple MFT predicted. Nevertheless, we obtained the fitted $g_{\perp}^{\text{cant}}$ close to 2.08 and |D/2J| equal to 0.05 rad, which is close to the value 0.04 rad as deduced from the $\Delta g/g$ calculation.

Spin Configuration. Although the detailed spin structure of these compounds will not be known until neutron diffraction studies are completed, it still is possible to postulate a reasonable picture of the spin array that is consistent with the structural and susceptibility results. These results have revealed a three-dimensional spin system. Such a spin array is shown in Figure 8, where the degree of canting, ϕ, is exaggerated for clarity. The array may be described as an almost simple cubic antiferromagnet in which the spins are coupled antiferromagnetically along all directions. As the susceptibility measurements show that the easy axis lies along the c direction and canting occurs only in the b direction, it is proposed that the spins are quantized in the c axis, but that they make an angle ϕ with the b axis of some 2°, rather than the 0° that occurs with a normal antiferromagnet. Because no weak ferromagnetic moment is detected in χ_a, the spins must lie in the bc plane, resulting in a small net moment along b.

Superexchange, as seen from these experiments, occurs in a three-dimensional network connecting the iron tetrahedra. The likely superexchange paths for these and similar compounds are explored in part 2 of this series.[35]

Acknowledgment. The work in Chicago was supported in part by the Solid State Chemistry Program of the Division of Materials Research of the National Science Foundation, under Grants DMR-8515224 and DMR-8815798. We also thank Basrah University and the Iraqi government for the award of a scholarship. Acknowledgement is made to the donors of the Petroleum Research Fund, administered by the American Chemical Society, for partial support of this research. Hau Wang at Argonne National Laboratory helped to obtain the EPR spectra.

Supplementary Material Available: Plots of (χ vs H)$_T$ (Figure S1) and (χ vs T)$_H$ (Figure S2) data curves for $C_{15}H_{15}Br_3Cl_9Fe_2N_3$ and tables of crystallographic parameters, fractional atomic coordinates for H atoms at calculated positions, and thermal parameters (6 pages); a table of structure factor amplitudes for $C_{15}H_{15}Cl_{12}Fe_2N_3$ (14 pages). Ordering information is given on any current masthead page.

(35) Lowe, C. B.; Carlin, R. L.; Loong, C.-K.; Schultz, A. J. *Inorg. Chem.*, following paper in this issue.

Contribution from the Department of Chemistry, University of Illinois at Chicago, Chicago, Illinois 60680, and Chemistry, Materials Science and Pulsed Neutron Divisions, Argonne National Laboratory, Argonne, Illinois 60439

Magnetochemistry of the Tetrahaloferrate(III) Ions. 2. Crystal Structure and Magnetic Ordering in [4-Br(py)H]$_3Fe_2Cl_{1.3}Br_{7.7}$ and [4-Cl(py)H]$_3Fe_2Br_9$. The Superexchange Paths in the $A_3Fe_2X_9$ Salts

Carol B. Lowe, Richard L. Carlin,* Arthur J. Schultz, and C.-K. Loong

Received December 14, 1989

A series of neutron diffraction investigations at 25 K are reported on single crystals of stoichiometry (4-chloropyridinium)$_3Fe_2Br_9$ and on (4-bromopyridinium)$_3Fe_2Cl_{1.3}Br_{7.7}$. The compound of stoichiometry (4-bromopyridinium)$_3Fe_2Cl_{1.3}Br_{7.7}$ is found to belong to the space group $P2_1/n$ with four formula units in the unit cell. Structural analysis shows that the iron is present as the [FeX_4]$^-$ ion (X = Cl, Br). The cell dimensions are a = 14.892 (3) Å, b = 14.184 (4) Å, c = 15.147 (4) Å, and β = 91.44 (2)°. The related compound (4-chloropyridinium)$_3Fe_2Br_9$ is found to belong to the same space group with a = 14.856 (3) Å, b = 14.066 (3) Å, c = 15.216 (3) Å, and β = 92.15 (1)°. Both materials are isomorphous with the previously reported bis[4-chloropyridinium tetrachloroferrate(III)]-4-chloropyridinium chloride. Magnetic measurements on single crystals show that the $S = {}^5/_2$ material (4-bromopyridinium)$_3Fe_2Cl_{1.3}Br_{7.7}$ orders as a canted antiferromagnet at 5.67 K, while (4-chloropyridinium)$_3Fe_2Br_9$ orders in a similar fashion at 7.96 K. Magnetic susceptibility data are compared with the theoretical predictions for the simple cubic (sc) Heisenberg high-temperature series expansion model, and superexchange pathways for the isostructural series of monoclinic $A_3Fe_2X_9$ salts are examined.

Introduction

This paper is the second in a series on some ferric compounds of stoichiometry $A_3Fe_2X_9$.[1] By comparison with a variety of other transition metal salts having this stoichiometry, one might expect to find binuclear [Fe_2X_9]$^{3-}$ ions in the crystal structure, but this has not been found to be true in these or other Fe(III) compounds of which we are aware. Rather, discrete, tetrahedral [FeX_4]$^-$ ions (X = Cl, Br) are found to be present. We report here the syntheses, the crystal structures, and the magnetic properties for the new mixed-halide compound [4-Br(py)H]$_3Fe_{1.3}Br_{7.7}$, and similar data for [4-Cl(py)H]$_3Fe_2Br_9$(4-X(py)H = 4-halo-

* To whom correspondence should be addressed at the University of Illinois at Chicago.

(1) Part 1: Zora, J. A.; Seddon, K. R.; Hitchcock, P. B.; Lowe, C. B.; Shum, D. P.; Carlin, R. L. *Inorg. Chem.*, preceding paper in this issue.

0020-1669/90/1329-3308$02.50/0

pyridinium). Both of these compounds appear to behave as canted antiferromagnets at low temperatures. These $S = {}^5/_2$ compounds are two of a large series of tetrahaloferrates that exhibit unusual magnetic behavior and are currently under extensive investigation.[1,2] The original work of Dzyaloshinsky[3,4] on Fe_2O_3 was the first report of canted antiferromagnetism in molecular compounds of the S-state ion, iron(III); however the $[FeX_4]^-$ salts appear to be the first reported examples of materials having canting interactions between discrete ions.

For the series $[4\text{-}X(py)H]_3Fe_2X_9$, where X = Cl, Br, or a mixture of the two, it has been previously noted[1] that replacement of chloride by bromide on the pyridinium ring leads to a small decrease in the ordering temperature, T_c, presumably because the larger bromine atom serves only to increase the distance between the metal centers, thus diminishing the strength of magnetic interactions. A much stronger effect on T_c is seen when bromide replaces chloride at the anionic sites producing $[FeBr_4]^-$, $[FeCl_xBr_{4-x}]^-$ and Br^-. An explanation for the enhancement in superexchange is that there is increased electron delocalization onto the more polarizable bromide, enabling more efficient overlap. The increase in the exchange constant, $|J|/k_B$, is roughly a factor of 4 on going from the 4-chloropyridinium-containing tetrachloride to the analogous tetrabromide. Similar, though smaller effects for isomorphous chloride- and bromide-containing compounds have been noted previously by Willett and his colleagues.[5] As expected, halide mixing at the tetrahaloferrate(III) site causes magnetic ordering in a temperature range intermediate between those of the fully substituted anions.

Experimental Section

Preparation of Bis[4-chloropyridinium tetrabromoferrate(III)]-4-Chloropyridinium Bromide. Small single crystals of $2[4\text{-Cl(py)H}][FeBr_4]\cdot[4\text{-Cl(py)H}]Br$ were obtained from K. R. Seddon and J. E. Nivet-Wyldbore, Sussex, New Brighton, England. In addition, large single crystals were synthesized and grown from aqueous acid solutions at UIC. Analyses, unless otherwise noted, were performed by Galbraith Laboratories, Knoxville, TN. Anal. Calcd for $C_{15}H_{15}Br_9Cl_3Fe_2N_3$: C, 15.34; H, 1.29; Br, 61.23; Cl, 9.06; Fe, 9.51; N, 3.58. Found: C, 15.29; H, 1.33; Br, 60.68; Cl, 9.37; Fe, 9.52; N, 3.56. Found (crystals, analyses from Sussex): C, 15.29; H, 1.24; N, 3.60.

Preparation of Bis[4-bromopyridinium tetrahaloferrate(III)]-4-Bromopyridinium Halide. (Halide is chloride, bromide in the ratio 1.3:7.7.) $FeCl_3\cdot 6H_2O$ in the amount of 8.15 g (0.030 mol) was dissolved in 15 mL of HBr (48%); 19.44 g (0.100 mol) of 4-bromopyridinium chloride was dissolved separately in 35 mL of HBr (48%) with a minimal amount of distilled water and gentle heating. The two solutions were subsequently mixed; the precipitate formed was filtered off and redissolved in 135 mL of slightly warm dilute HBr. When the solution was left for several weeks at room temperature over sulfuric acid, large black single crystals (dark red when pulverized) were formed, suitable for magnetic and neutron diffraction measurements. Anal. Calcd for $C_{15}H_{15}Br_{10.7}Cl_{1.3}Fe_2N_3$: C, 14.41; H, 1.21; **Br**, 68.39; Cl, 3.69; Fe, 8.94; N, 3.36. Found: C, 14.38; H, 1.23; **Br**, 68.40; Cl, 4.62; Fe, 9.11; N, 3.24.

Single-Crystal Neutron Analysis. Time-of-flight (TOF) neutron diffraction data were obtained at the Intense Pulsed Neutron Source (IPNS) at Argonne National Laboratory. The experiments were performed by using a single-crystal diffractometer (SCD) equipped with an area position-sensitive ^{6}Li glass scintillation detector and an Air Products Displex closed-cycle helium refrigerator for cooling the sample. Details of the data collection and analysis procedures have been previously provided.[6] Table I contains a summary of the data collection, analysis and refinement parameters for $[4\text{-Br(py)H}]_3Fe_2Cl_{1.3}Br_{7.7}$. Twenty-four crystal orientations were required to cover a unique quadrant of reciprocal space. For each crystal setting, data were stored in three-dimensional histogram form with coordinates x,y,t corresponding to horizontal and vertical detector positions and the TOF, respectively. The 120 TOF histogram channels were constructed with constant $\Delta t/t = 0.015$ (where Δt is the channel width) and correspond to wavelengths of 0.7–4.2 Å as given by the de Broglie equation $\lambda = (h/m)(t/L)$, where h is Planck's constant, m is the neutron mass, and t is the TOF for the total flight path length L.

Table I. Crystallographic Data for $[4\text{-Br(py)H}]_3Fe_2Cl_{1.3}Br_{7.7}$ and $[4\text{-Cl(py)H}]_3Fe_2Br_9$

chem formula	$C_{15}H_{15}Cl_{1.3}Br_{10.7}Fe_2N_3$	$C_{15}H_{15}Br_9Cl_3Fe_2N_3$
fw	1250.1	1174.5
space group	$P2_1/n$ (No. 14)	$P2_1/n$ (No. 14)
T, K	25	25
a, Å	14.892 (3)	14.856 (3)
b, Å	14.184 (4)	14.066 (4)
c, Å	15.147 (3)	15.216 (3)
β, deg	91.44 (2)	92.15 (1)
V, Å^3	3198 (1)	3177 (1)
Z	4	4
λ range, Å	0.7–4.2 Å	0.7–4.2 Å
ρ_{calcd}, g/cm^3	2.596	2.455
μ(0.7 Å), cm^{-1}	0.7136	0.7482
μ(4.2 Å), cm^{-1}	2.286	2.445
$R(F)$	0.049	0.0507
$R(F^2)$	0.083	0.0877
$R_w(F^2)$	0.073	0.0819
GOF	1.571	1.840

Initially, an orientation matrix was obtained by an autoindexing procedure[7] using data obtained by searching a histogram for peaks. Bragg reflections were integrated about their predicted histogram location and were corrected for the Lorentz factor, the incident spectrum, the detector efficiency, dead-time losses, and crystal absorption.[6,8] The initial coordinates for the non-hydrogen atoms were those from the X-ray structure of bis[4-chloropyridinium tetrachloroferrate(III)]-4-chloropyridinium chloride.[1] After several cycles of least-squares refinement, hydrogen atoms were located in a difference Fourier map using phases calculated from the non-hydrogen atomic coordinates. Atomic scattering lengths used in the least-squares refinements were those tabulated by Sears[9] except for the 12 bromine/chlorine atoms for which the scattering lengths were treated as variables. In the final cycles of least-squares refinements, all atoms were treated with anisotropic temperature factors and a secondary extinction correction was included. Table II contains the final atomic coordinates and the Br/Cl distribution derived from the refined scattering lengths ($b_{Cl} = 0.9577$, $b_{Br} = 0.6795$ in units of 10^{-12} cm). For convenience, all Br/Cl atoms are labeled Br. Anisotropic temperature factors and observed and calculated structure factors are given in the supplementary material.

Susceptibility Measurements. Measurement of the zero-field susceptibility of single crystals and polycrystalline powders from 2 to 40 K was carried out using an ac susceptometer previously described.[10] Data were obtained by the same ac technique for lower temperatures (1–4.2 K), by using another apparatus.[4] The operating frequency for these experiments was 175 Hz. Both in- and out-of-phase components of the susceptibility were monitored throughout the range of measurements, and the reference material cerium(III) magnesium nitrate was employed as a standard.

Results

Crystal Structure. A. $[4\text{-Br(py)H}]_3Fe_2Cl_{1.3}Br_{7.7}$. The crystal unit cell for $[4\text{-Br(py)H}]_3Fe_2Cl_{1.3}Br_{7.7}$ is shown in Figure 1. A double salt is defined by the asymmetric unit, which contains three 4-bromopyridinium cations, two $[FeX_4]^-$ anions and one Br^- anion. The tetrahedral $[FeX_4]^-$ units are spaced unevenly in an alternating fashion along the crystallographic c axis, with four of these asymmetric subsets per unit cell, with the large organic pyridinium rings and lone halide anions interspersed.

No long-range hydrogen-bonding network is evident from the structure; instead, we see that each Br^- anion, Br(12), has three short pyridinium ring N–H···Br(12) hydrogen bonds and one C–H···Br(12) contact, which produces a centrosymmetric ring linking two Br(12) anions to form discrete dimers. This config-

(2) (a) Lowe, C. B.; Carlin, R. L.; Schultz, A. J.; Loong, C.-K.; Zora, J. A.; Seddon, K. R.; Hitchcock, P. B.; Lammers, E.; van Duyneveldt, A. J. Unpublished material. (b) Lammers, E.; Verstelle, J. C.; van Duyneveldt, A. J.; Lowe, C.; Carlin, R. L. *J. Phys. (Paris)* **1988**, *49*, 1465.
(3) Dzyaloshinsky, I. *J. Phys. Chem. Solids* **1958**, *4*, 241.
(4) Carlin, R. L. *Magnetochemistry*; Springer-Verlag: Berlin, Heidelberg, FRG, New York, Tokyo, 1986.
(5) Willett, R. D. *J. Am. Chem. Soc.* **1988**, *110*, 8639.
(6) (a) Schultz, A. J.; Srinivansan, K.; Teller, R. G.; Williams, J. M.; Lukehart, C. M. *J. Am. Chem. Soc.* **1984**, *106*, 999. (b) Schultz, A. J.; Leung, P. C. W. *J. Phys. (Les Ulis, Fr.)*, Colloq. *C5* **1986**, *47*, C5-137. (c) Schultz, A. J. *Trans. Am. Crystallogr. Assoc.* **1988**, *23*, 61.
(7) Jacobson, R. A. *J. Appl. Crystallogr.* **1986**, *19*, 283.
(8) Howard, J. A. K.; Johnson, O.; Schultz, A. J., Stringer, A. M. *J. Appl. Crystallogr.* **1987**, *20*, 120.
(9) Sears, V. F. in *Neutron Scattering*; Skold, K.; Price, D. L., Eds., Methods of Experimental Physics 23, Part A; Academic Press: Orlando, FL, 1986; pp 521–550.
(10) McElearney, J. N.; Losee, D. B.; Merchant, S.; Carlin, R. L. *Phys. Rev.* **1973**, *B7*, 3314.

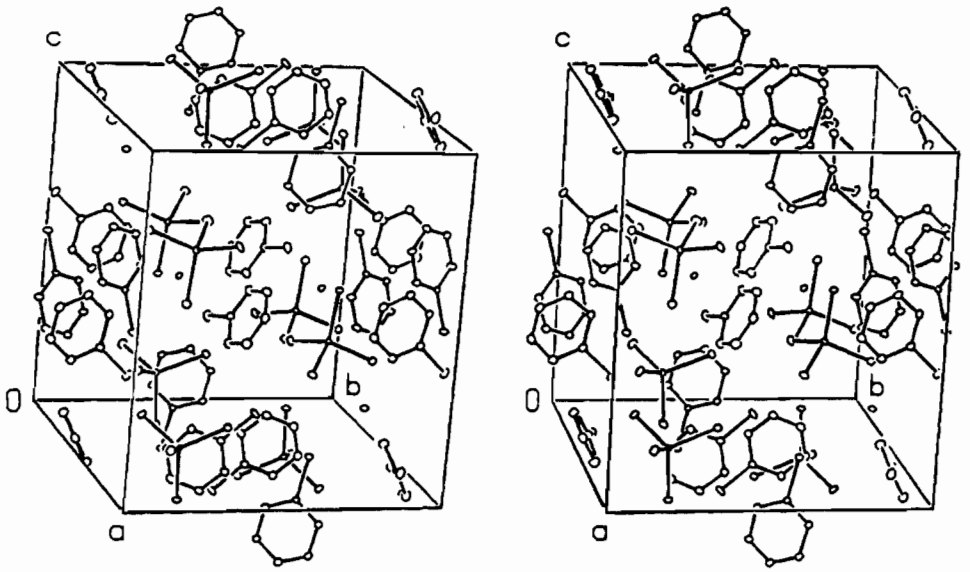

Figure 1. Stereoview of the unit cell of $[4\text{-Br(py)H}]_3Fe_2Cl_{1.3}Br_{7.7}$ with thermal ellipsoids drawn at the 50% probability level. For reasons of clarity, hydrogen atoms are not shown.

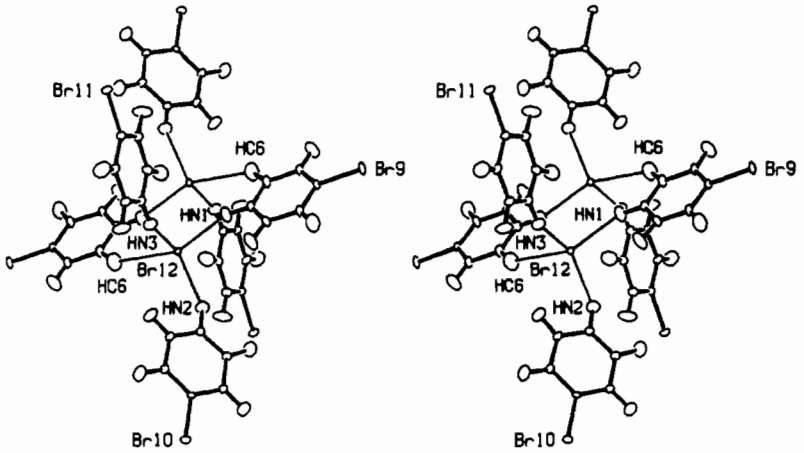

Figure 2. Stereoview of the H···Br(12) hydrogen-bonding interactions. See Table IIIc for distances.

uration is illustrated in Figure 2; the H···Br(12) contacts are given in Table III.

Intramolecular bond distances for the halo-substituted pyridinium cation are comparable to literature values, with averages of 1.390 Å for C–C, 1.344 Å for C–N, 1.082 Å for C–H, 1.871 Å for C–Br and 1.031 Å for N–H. Pyridinium bond angles also appear normal for the planar system.

The Cl/Br distribution given in Table II shows that pyridinium bromines, Br(9), Br(10), and Br(11), and the bromine anion, Br(12), have no chlorine occupancy within experimental error. Thus, the chlorines are distributed about the iron coordination spheres mostly on the Br(3) site about Fe(1) and on the Br(7) site about Fe(2). As shown in Table IV, the eight observed Fe–Br distances vary linearly (from 2.280 (2) to 2.349 (2) Å) with the fractional occupancy of bromine. Of course, these observed bond lengths result from fitting static random disorder of partially occupied chlorine and bromine atoms with a single atom, and therefore, they do not correspond to true interatomic bond distances. $[FeX_4]^-$ bond angles range from 106.87 (7) to 111.95 (7)°, indicating little distortion from the regular 109.5° tetrahedral angle.

B. $[4\text{-Cl(py)H}]_3Fe_2Br_9$. The compound $[4\text{-Cl(py)H}]_3Fe_2Br_9$ is isostructural with both $[4\text{-Br(py)H}]_3Fe_2Cl_{1.3}Br_{7.7}$ and $[4\text{-Cl(py)H}]_3Fe_2Cl_9$. The crystal packing illustrated in Figure 1 for $[4\text{-Br(py)H}]_3Fe_2Cl_{1.3}Br_{7.7}$ is representative for the series. The iron(III) tetrahedra in the asymmetric unit are aligned pairwise along *c*; their 3-fold axes are nearly coincident with the *c* crystallographic direction. Intra- and intermolecular iron–iron distances along the *c* axis differ by about 1 Å and the angle Fe(1)···X(6)–Fe(2) is not far from linear at approximately 167°.

Hydrogen-bonding interactions for $[4\text{-Cl(py)H}]_3Fe_2Br_9$ are similar to those pictured for the mixed tetrahalide salt; these contacts, as well as intramolecular bond distances and angles for $[4\text{-Cl(py)H}]_3Fe_2Br_9$ are given in Table V and the supplementary Table S6, respectively.

Superexchange Pathways. Potential superexchange pathways examined for these salts are of three general types, each involving halide as the intervening anion. All else being equal, a difference in magnetic coupling between the same spin state compounds with similar coordination depends upon the amount of overlap, which is governed by the particular intervening anion enabling the interaction, the angle of overlap M–L···(L)–M, and the distances and geometry along the compared pathways.[11] Recent studies demonstrate that the shortest intermetal distance does not always determine the strongest magnetic coupling within a compound, and in fact moderately strong intramolecular superexchange interactions have been shown between Cu(II) ions separated by more than 11 Å. The molecules were designed with large bridging terephthalato ligands coplanar to the two metal centers of the dimer, and although substantially shorter interdimer Cu···Cu distances were found, magnetic interactions between separate dinuclear units were ruled out by using crystal packing arguments.[12] Because no bridging ligands are present in the com-

(11) Blanchette, J. T.; Willett, R. D. *Inorg. Chem.* **1988**, *27*, 843.

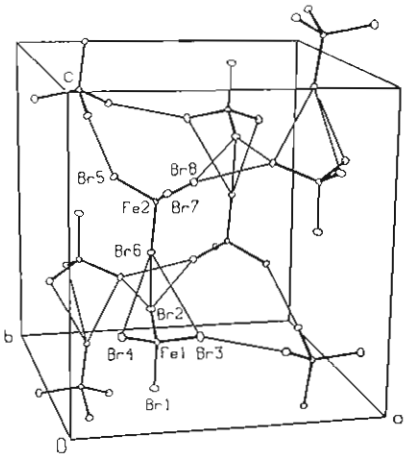

Figure 3. Perspective drawing of a unit cell with only the $[FeBr_4]^-$ anions. Br···Br contacts of less than 5.0 Å, ranging from Br(4)···Br(8) = 3.794 (2) Å to Br(3)···Br(6) = 4.446 (2) Å, are shown as thin lines.

pounds described here and some previous serial studies of superexchange interactions do correlate strongly to distance ($\propto r^{-12}$ for the $S = {}^5/_2$ ions in $AMnF_3$ and A_2MnF_4 manganese fluorides),[13] attention was focused first on short interion halide–halide contacts for each of the compounds $[4\text{-Cl(py)H}]_3\{FeCl_4\}_2Cl$, $[4\text{-Br(py)H}]_3[FeCl_xBr_{4-x}]_2Br$ ($x = 0.65$), and $[4\text{-Cl(py)H}]_3[FeBr_4]_2Br$.

The free halide, Br(12), with its four hydrogen bonds to pyridinium ring hydrogens, is surrounded and effectively insulated from close contact with other halides and the superexchange pathways. As given in Tables III and V, the shortest interhalide distances include many of the pyridinium ring halides, giving possible type I Fe–X···X⁻···X–Fe interactions, but then the total exchange path length becomes rather long (exceeding 10 Å), for the noncoplanar nonbridging path geometry. Although contributions from five-center pathways may not now be ruled out, these offer seemingly no advantage over another interaction path, which is shorter and has fewer intervening anions. A roughly three-dimensional network of Fe–X···X–Fe nearest interactions (type II) is obtained using an arbitrary cutoff at about 5 Å for the interhalide distance, as shown in Figure 3. A compilation of calculated total superexchange pathlengths is given in Table VI. Three different paths are drawn between Fe(1) and Fe(2) parallel to the *c* axis, these iron atoms being the inequivalent pair in the asymmetric unit. No other multiple interactions between neighboring metal ions are evident; each has but a single exchange path to another metal atom extending generally into the *a* and *b* crystallographic directions.

A third type of pathway, connecting the iron atoms of each asymmetric unit and having but one intervening halide ligand was considered (Figure 4). Total path lengths of between 6.0 and 6.6 Å for Fe(1)···X(6)–Fe(2) are observed, depending on the particular compound; however, no favorable magnetic overlap is available between the aligned nonorthogonal tetrahedrally hybridized Fe orbital and the axially directed anion, and therefore, this path (type III) will be neglected.

Magnetic Susceptibility. A. $[4\text{-Cl(py)H}]_3Fe_2Br_9$. Susceptibility data for $[4\text{-Cl(py)H}]_3Fe_2Br_9$, as shown in Figure 5, indicate three-dimensional antiferromagnetic ordering at 7.96 K. A weak ferromagnetic peak is distinct at T_c in measurements taken along the *b* crystallographic axis and is weakly evident in the *a* axis data, probably due to misalignment of the crystal for this measurement. A sharp change in the quadrature or out-of-phase χ'' signal accompanying the peak in χ along *b* is evidenced only in the narrow temperature region between 7.7 and 8.0 K. Data collected with the applied field parallel to the *a* and *c* directions show normal antiferromagnetic (AF) behavior, *c* being the easy axis. Powder

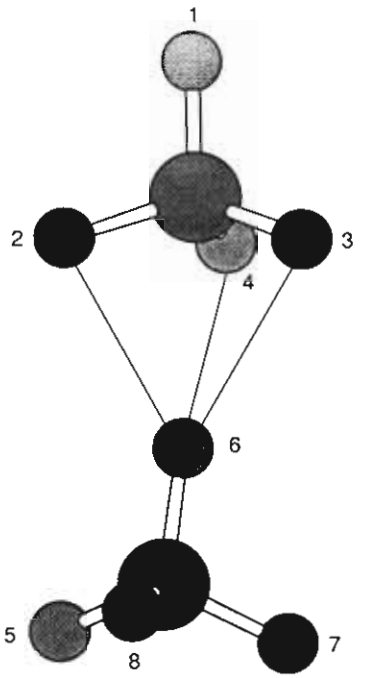

Figure 4. Important superexchange contacts (types II) within the asymmetric unit of the unit cell.

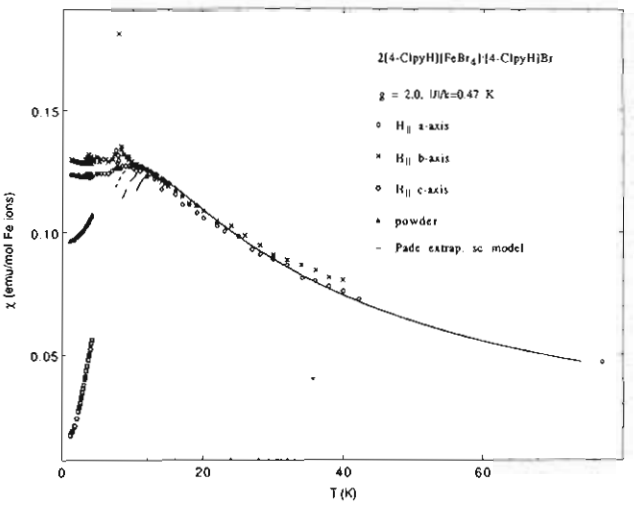

Figure 5. Magnetic susceptibility data for $[4\text{-Cl(py)H}]_3Fe_2Br_9$. The solid line is the Padé approximant to the χ HTS expansion. Longer dashes indicate the χ expansion including all eight available terms; shorter dashes are same with only six terms included.

data collected in the range 1.1 to 4.2 K are also shown. The solid curve is the theoretical result for an $S = {}^5/_2$ simple cubic (sc) Heisenberg AF with $|J|/k_B = 0.47$ K and $g = 1.98$, obtained by using Padé approximants ($\gamma = 1.405$) to extrapolate results of the high-temperature series expansion (HTS) in χ to lower temperature.[14] The dashed line is the normal HTS expansion of the χ expression previously given[15] using eight available terms. The dotted line is the HTS expansion using only the first six terms of the series.

B. $[4\text{-Br(py)H}]_3Fe_2Cl_{1.3}Br_{7.7}$. Figure 6 gives the results for similarly measured $[4\text{-Br(py)H}]_3Fe_2Cl_xBr_{9-x}$, with alignment as indicated. Along the *a* direction (Figure 6a), we see two well-defined weak ferromagnetic peaks (a change in the χ'' out-of-phase signal was noted for both). In the *b* and *c* directions (Figure 6b,c), more intense, less well-defined peaks are observed. The easy axis, if one might be so named, is in this case along the *b* axis direction.

(12) Chaudhuri, P.; Oder, K.; Wieghardt, K.; Gehring, S.; Haase, W.; Nuber, B.; Weiss, J. *J. Am. Chem. Soc.* **1988**, *110*, 3657.
(13) de Jongh, L. J.; Block, R. *Physica* **1975**, *79B*, 568.
(14) Navarro, R. Thesis, Universidad de Zaragoza, 1976, unpublished.
(15) Rushbrooke, G. S.; Wood, P. J. *J. Mol. Phys.* **1958**, *1*, 257.

Table II. Atomic Parameters for $[4\text{-Br(py)H}]_3Fe_2Cl_{1.3}Br_{7.7}$ and $[4\text{-Cl(py)H}]_3Fe_2Br_9$ at 25 K from Neutron Diffraction Data

a. $[4\text{-Br(py)H}]_3Fe_2Cl_{1.3}Br_{7.7}$

atom	x	y	z	U_{eq},[a] Å^2	% Br[b]	atom	x	y	z	U_{eq},[a] Å^2
Fe(1)	0.32949 (7)	0.28566 (8)	0.18299 (7)	0.0086 (3)		C(9)	0.8920 (1)	0.5760 (1)	−0.0077 (1)	0.0089 (5)
Fe(2)	0.32526 (7)	0.28679 (8)	0.62249 (7)	0.0077 (3)		C(10)	0.8536 (1)	0.4924 (1)	−0.0397 (1)	0.0115 (5)
Br(1)	0.3258 (1)	0.2999 (1)	0.0303 (1)	0.0148 (6)	88 (2)	C(11)	0.8619 (1)	0.4709 (1)	−0.1282 (1)	0.0128 (5)
Br(2)	0.3446 (1)	0.4380 (1)	0.2420 (1)	0.0140 (6)	95 (2)	C(12)	0.0693 (1)	0.2389 (1)	0.5349 (1)	0.0135 (6)
Br(3)	0.4468 (1)	0.1904 (1)	0.22469 (9)	0.0136 (5)	66 (2)	C(13)	0.0845 (1)	0.1691 (1)	0.5975 (1)	0.0139 (5)
Br(4)	0.1999 (1)	0.2129 (1)	0.2293 (1)	0.0150 (6)	89 (2)	C(14)	0.1009 (1)	0.0777 (1)	0.5683 (1)	0.0112 (5)
Br(5)	0.2090 (1)	0.3724 (1)	0.68195 (9)	0.0131 (6)	85 (2)	C(15)	0.1023 (1)	0.0575 (1)	0.4778 (1)	0.0142 (6)
Br(6)	0.3068 (1)	0.2735 (1)	0.46854 (9)	0.0103 (5)	98 (2)	C(16)	0.0864 (1)	0.1305 (1)	0.4186 (1)	0.0146 (5)
Br(7)	0.32452 (9)	0.1380 (1)	0.67934 (9)	0.0122 (5)	63 (2)	H(N1)	0.3805 (2)	0.0250 (3)	1.0053 (2)	0.028 (1)
Br(8)	0.4624 (1)	0.3574 (1)	0.6607 (1)	0.0133 (6)	93 (2)	H(N2)	0.5866 (2)	0.0155 (3)	0.7472 (2)	0.025 (1)
Br(9)	0.5275 (1)	0.3705 (1)	0.4086 (1)	0.0133 (6)	100 (2)	H(N3)	0.0611 (2)	0.2743 (3)	0.4061 (2)	0.027 (1)
Br(10)	0.8814 (1)	0.6081 (1)	0.1113 (1)	0.0136 (6)	101 (2)	H(C2)	0.7295 (3)	0.0130 (3)	0.8978 (3)	0.036 (1)
Br(11)	0.1203 (1)	−0.0170 (1)	0.6525 (1)	0.0155 (6)	102 (2)	H(C3)	0.1098 (3)	0.0321 (3)	0.0652 (3)	0.035 (1)
Br(12)	0.0362 (1)	0.4326 (1)	0.38427 (9)	0.0085 (5)	96 (2)	H(C5)	0.2027 (3)	0.1552 (3)	0.8239 (2)	0.036 (1)
N(1)	0.81666 (9)	0.45341 (9)	0.48743 (8)	0.0135 (4)		H(C6)	0.3593 (3)	0.1053 (3)	0.8715 (3)	0.039 (1)
N(2)	0.90633 (8)	0.53025 (9)	−0.18095 (8)	0.0114 (4)		H(C7)	0.5226 (3)	0.1532 (3)	0.7000 (2)	0.033 (1)
N(3)	0.07059 (8)	0.2181 (1)	0.44849 (8)	0.0129 (4)		H(C8)	0.5325 (3)	0.2013 (3)	0.5397 (2)	0.036 (1)
C(2)	0.7507 (1)	0.4748 (1)	0.5426 (1)	0.0134 (5)		H(C10)	0.3190 (3)	0.0552 (3)	0.5030 (2)	0.031 (1)
C(3)	0.6629 (1)	0.4503 (1)	0.5213 (1)	0.0137 (5)		H(C11)	0.3342 (3)	0.0924 (3)	0.3412 (2)	0.035 (1)
C(4)	0.6455 (1)	0.4036 (1)	0.4416 (1)	0.0092 (5)		H(C12)	0.5553 (3)	0.1880 (3)	0.0515 (2)	0.034 (1)
C(5)	0.7148 (1)	0.3812 (1)	0.3858 (1)	0.0138 (5)		H(C13)	0.0829 (3)	0.1863 (3)	0.6670 (2)	0.036 (1)
C(6)	0.8014 (1)	0.4078 (1)	0.4105 (1)	0.0160 (6)		H(C15)	0.8842 (3)	0.0124 (3)	0.5467 (3)	0.035 (1)
C(7)	0.9437 (1)	0.6106 (1)	−0.1517 (1)	0.0127 (5)		H(C16)	0.0861 (3)	0.1210 (3)	0.3479 (2)	0.036 (1)
C(8)	0.9379 (1)	0.6358 (1)	−0.0634 (1)	0.0138 (5)						

b. $[4\text{-Cl(py)H}]_3Fe_2Br_9$

atom	x	y	z	U_{eq},[a] Å^2	atom	x	y	z	U_{eq},[a] Å^2
Fe(1)	0.33576 (8)	0.2864 (1)	0.18830 (8)	0.0094 (4)	C(9)	0.8906 (1)	0.5805 (2)	−0.0088 (1)	0.0132 (6)
Fe(2)	0.32764 (8)	0.2872 (1)	0.63115 (8)	0.0099 (4)	C(10)	0.8547 (1)	0.4939 (2)	−0.0389 (1)	0.0142 (6)
Br(1)	0.3280 (1)	0.2955 (2)	0.0348 (1)	0.0168 (6)	C(11)	0.8631 (1)	0.4709 (2)	−0.1263 (1)	0.0157 (6)
Br(2)	0.3500 (1)	0.4419 (2)	0.2430 (1)	0.0176 (6)	C(12)	0.0718 (1)	0.2377 (2)	0.5373 (1)	0.0154 (7)
Br(3)	0.4590 (1)	0.1931 (2)	0.2330 (1)	0.0170 (6)	C(13)	0.0902 (1)	0.1650 (2)	0.5967 (1)	0.0154 (6)
Br(4)	0.2064 (1)	0.2119 (2)	0.2374 (1)	0.0205 (6)	C(14)	0.1043 (1)	0.0740 (2)	0.5643 (1)	0.0127 (6)
Br(5)	0.2100 (1)	0.3712 (2)	0.6928 (1)	0.0162 (6)	C(15)	0.1000 (1)	0.0566 (2)	0.4738 (1)	0.0154 (7)
Br(6)	0.3087 (1)	0.2758 (2)	0.4778 (1)	0.0145 (6)	C(16)	0.0814 (1)	0.1319 (2)	0.4178 (1)	0.0160 (7)
Br(7)	0.3287 (1)	0.1313 (2)	0.6855 (1)	0.0149 (6)	H(N1)	0.3768 (3)	0.0203 (4)	1.0084 (3)	0.032 (1)
Br(8)	0.4650 (1)	0.3613 (2)	0.6704 (1)	0.0155 (6)	H(N2)	0.5873 (3)	0.0152 (4)	0.7448 (3)	0.031 (2)
Cl(9)	0.53186 (8)	0.3711 (1)	0.4193 (1)	0.0186 (5)	H(N3)	0.0563 (3)	0.2776 (4)	0.4102 (3)	0.029 (1)
Cl(10)	0.8810 (1)	0.6114 (1)	0.09893 (9)	0.0225 (5)	H(C2)	0.7315 (3)	0.0130 (4)	0.8935 (3)	0.039 (2)
Cl(11)	0.1260 (1)	−0.0171 (1)	0.6368 (1)	0.0202 (5)	H(C3)	0.1072 (3)	0.0339 (4)	0.0720 (3)	0.043 (2)
Br(12)	0.0342 (1)	0.4342 (1)	0.3824 (1)	0.0128 (6)	H(C5)	0.1953 (3)	0.1508 (4)	0.8281 (3)	0.042 (2)
N(1)	0.81232 (9)	0.4578 (1)	0.4907 (1)	0.0147 (5)	H(C6)	0.3535 (3)	0.0985 (4)	0.8741 (3)	0.040 (2)
N(2)	0.90504 (9)	0.5311 (1)	−0.1799 (1)	0.0138 (5)	H(C7)	0.5286 (3)	0.1578 (4)	0.7011 (3)	0.034 (2)
N(3)	0.06807 (8)	0.2194 (1)	0.4504 (1)	0.0143 (5)	H(C8)	0.5392 (3)	0.2091 (4)	0.5433 (3)	0.041 (2)
C(2)	0.7472 (1)	0.4767 (2)	0.5469 (1)	0.0166 (7)	H(C10)	0.3225 (3)	0.0548 (4)	0.5050 (3)	0.035 (2)
C(3)	0.6590 (1)	0.4503 (2)	0.5267 (1)	0.0158 (7)	H(C11)	0.3370 (3)	0.0947 (4)	0.3447 (3)	0.040 (2)
C(4)	0.6404 (1)	0.4043 (2)	0.4473 (1)	0.0119 (6)	H(C12)	0.5600 (3)	0.1893 (4)	0.0562 (3)	0.036 (2)
C(5)	0.7092 (1)	0.3844 (2)	0.3900 (1)	0.0161 (7)	H(C13)	0.0943 (3)	0.1804 (4)	0.6663 (3)	0.037 (2)
C(6)	0.7961 (1)	0.4128 (2)	0.4138 (1)	0.0186 (7)	H(C15)	0.8885 (3)	0.0140 (4)	0.5524 (3)	0.037 (2)
C(7)	0.9395 (1)	0.6150 (2)	−0.1522 (1)	0.0141 (6)	H(C16)	0.0757 (3)	0.1240 (4)	0.3472 (3)	0.038 (2)
C(8)	0.9332 (1)	0.6416 (2)	−0.0652 (1)	0.0156 (7)					

[a] Equivalent isotropic U defined as $^1/_3 \sum_i \sum_j U_{ij}\, a_i^* a_j^* \mathbf{a}_i \cdot \mathbf{a}_j$. [b] Percent bromine derived from refinement of the atomic scattering length. Percent chlorine occupancy is % Cl = 100 − % Br.

As this curve does not approach the origin directly, there may be either misalignment or else contributions from nonuniform spin alignments or from contaminating $[FeBr_2Cl_2]^-$, $[FeBrCl_3]^-$, or even $[FeCl_4]^-$ species in the lattice.

Curie–Weiss analysis in the paramagnetic region gives $g = 2.08$. No comparison to a model curve is given here, due to the complication that weak ferromagnetic peaks appear at more than one temperature, making it difficult to define the parameters T_c, χ_{max}, and $T(\chi_{max})$. The primary canting peak seen from the b axis susceptibility measurement in Figure 6b appears at 5.67 K.

Discussion

Structural and Crystallographic Correlations. The three isostructural compounds of stoichiometry $A_3Fe_2X_9$ arranged in order of increasing cell volumes are as follows: $[4\text{-Cl(py)H}]_3Fe_2Cl_9$ < $[4\text{-Cl(py)H}]_3Fe_2Br_9$ < $[4\text{-Br(py)H}]_3Fe_2Cl_{1.3}Br_{7.7}$. The parameters a and b for the compounds ascend in this order as well, a condition that relates primarily to the change of ring substituent from Cl to Br. However the c axis is longest for $[4\text{-Cl(py)H}]_3Fe_2Br_9$, where the Fe tetrahedra are statistically fully brominated. We recall that the Fe(2) tetrahedron most closely approaches Fe(1) along its 3-fold axis parallel to c. Since one axial halide site which points along c, X(1), in the mixed halide salt has a 12% preference for occupation by Cl, an intermediate value of c is the expected result.

Only two other crystal structure determinations of compounds containing the discrete $[FeBr_4]^-$ anion are known to us from the literature. Of these, the orthorhombic structure of $(H_3CNH_3)_2[FeBr_4]Br$, which is another double salt, also contains two independent forms of tetrahedral tetrabromoferrate(III).[16] One of these tetrahedra exhibits one anomalously low value for the Fe–Br bond length that is not seen in any of the structures, $[4\text{-X(py)H}]_3Fe_2X_9$ (X = Cl, Br), known to us. The effect of this shorter bond on magnetic ordering is impossible to predict.

The other reported structure, that of 4-ethylpyridinium tetrabromoferrate(III),[17] contains a similar 4-substituted pyridinium

(16) Sproul, G. D.; Stucky, G. D. *Inorg. Chem.* **1972**, *11*, 1650.

Table III. Br···Br and H···Br Contacts (Å)[a]

a. Intermolecular Fe–Br···Br–Fe Interactions (<5.0 Å)			
Br(2)–Br(4)	3.980 (3)	Br(3)–Br(6)	4.446 (2)
Br(2)–Br(6)	4.199 (2)	Br(4)–Br(8)	3.794 (2)
Br(2)–Br(8)	4.317 (2)	Br(4)–Br(6)	4.015 (2)
Br(3)–Br(5)	4.073 (2)	Br(5)–Br(7)	4.348 (2)
b. Br(1) to Br(8) Contacts with Br(9) to Br(12) (<5.0 Å)			
Br(1)–Br(11)	3.894 (2)	Br(5)–Br(12)	4.669 (2)
Br(1)–Br(10)	3.935 (2)	Br(6)–Br(9)	3.697 (2)
Br(2)–Br(9)	3.790 (2)	Br(6)–Br(12)	4.766 (2)
Br(2)–Br(11)	4.498 (3)	Br(7)–Br(10)	3.742 (2)
Br(3)–Br(10)	3.710 (2)	Br(7)–Br(11)	3.766 (2)
Br(3)–Br(9)	3.945 (2)	Br(7)–Br(12)	4.481 (2)
Br(3)–Br(12)	4.022 (2)	Br(8)–Br(11)	3.588 (2)
Br(4)–Br(12)	4.633 (3)	Br(8)–Br(9)	3.968 (2)
Br(5)–Br(10)	3.450 (2)	Br(8)–Br(9)	4.003 (2)
Br(5)–Br(11)	3.859 (2)		
c. H···Br(12) Contacts			
H(N1)–Br(12)	2.439 (4)	H(N3)–Br(12)	2.299 (4)
H(N2)–Br(12)	2.344 (4)	H(C6)–Br(12)	2.691 (4)

[a] Br(1) to Br(4) are coordinated to Fe(1). Br(5) to Br(8) are coordinated to Fe(2). Br(9), Br(10), and Br(11) are bonded to pyridinium rings at the 4-position, across from N(1), N(2), and N(3), respectively. Br(12) is the "free" bromine anion.

Table IV. Intramolecular Fe–Br Distances (Å)

atoms	f(Br)[a]	obsd	calcd[b]	diff
Fe(1)–Br(1)	0.88 (2)	2.321 (2)	2.325	−0.004
Fe(1)–Br(2)	0.95 (2)	2.347 (2)	2.338	0.009
Fe(1)–Br(3)	0.66 (2)	2.285 (2)	2.283	0.002
Fe(1)–Br(4)	0.89 (2)	2.313 (2)	2.327	−0.014
Fe(2)–Br(5)	0.85 (2)	2.315 (2)	2.319	−0.004
Fe(2)–Br(6)	0.98 (2)	2.349 (2)	2.344	0.005
Fe(2)–Br(7)	0.63 (2)	2.280 (2)	2.278	−0.002
Fe(2)–Br(8)	0.93 (2)	2.335 (2)	2.335	0.000

[a] Fraction bromine derived from refined scattering length, where f(Br) + f(Cl) = 1.00. [b] Calculated from the linear equation d(Fe–Br) = 2.158 + 0.1898f(Br).

Table V. Br···Br and H···Br Contacts (Å) for $[4\text{-Cl(py)H}]_3Fe_2Br_9$[a]

a. Intermolecular Fe–Br···Br–Fe interactions (<5.0 Å)			
Br(2)–Br(4)	3.902 (3)	Br(3)–Br(6)	4.565 (3)
Br(2)–Br(6)	4.332 (3)	Br(4)–Br(8)	3.833 (3)
Br(2)–Br(8)	4.084 (3)	Br(4)–Br(6)	4.010 (3)
Br(3)–Br(5)	3.907 (3)	Br(5)–Br(7)	4.149 (3)
b. Br(1) to Br(8) contacts with Br(9) to Br(12) (<5.0 Å)			
Br(1)–Br(11)	3.791 (3)	Br(5)–Br(12)	4.653 (3)
Br(1)–Br(10)	3.876 (2)	Br(6)–Br(9)	3.715 (2)
Br(2)–Br(9)	3.866 (2)	Br(6)–Br(12)	4.822 (3)
Br(2)–Br(11)	4.587 (3)	Br(7)–Br(10)	3.751 (3)
Br(3)–Br(10)	3.613 (2)	Br(7)–Br(11)	3.716 (3)
Br(3)–Br(9)	3.904 (3)	Br(7)–Br(12)	4.296 (3)
Br(3)–Br(12)	4.046 (3)	Br(8)–Br(11)	3.696 (3)
Br(4)–Br(12)	4.649 (3)	Br(8)–Br(9)	3.986 (3)
Br(5)–Br(10)	3.499 (3)	Br(8)–Br(9)	4.004 (3)
Br(5)–Br(11)	3.838 (2)		
c. H···Br(12) Contacts			
H(N1)–Br(12)	2.410 (5)	H(N3)–Br(12)	2.265 (6)
H(N2)–Br(12)	2.373 (5)	H(C6)–Br(12)	2.722 (5)

[a] Br(1) to Br(4) are coordinated to Fe(1). Br(5) to Br(8) are coordinated to Fe(2). Br(9), Br(10), and Br(11) are bonded to pyridinium rings at the 4-position, across from N(1), N(2), and N(3), respectively. Br(12) is the "free" bromine anion.

cation, and crystallizes in the space group $P2_1/c$. The unit cell of this compound with stoichiometry $[4\text{-}C_2H_5(py)H][FeBr_4]$ has roughly half the volume of the 4-halopyridinium tetrahaloferrate(III) unit cells; notably, the cell is half as long only in the a dimension. In contrast to the salts of this paper, stability of this structure is provided by a single N–H···Br(4) hydrogen bond,

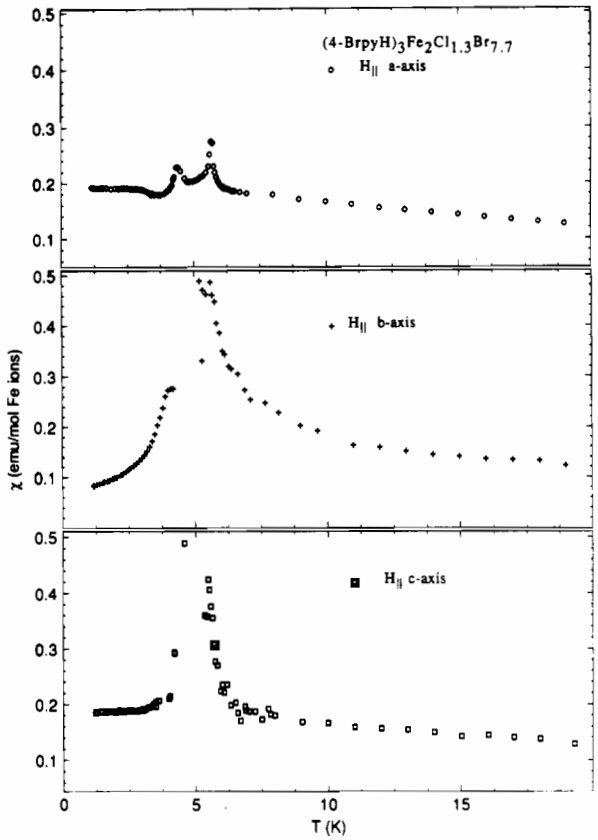

Figure 6. Single-crystal susceptibility data along three directions for $[4\text{-Br(py)H}]_3Fe_2Cl_{1.3}Br_{7.7}$.

which may be responsible for a slight distortion of the $[FeBr_4]^-$ tetrahedra. Here too the $[FeBr_4]^-$ tetrahedra are nearly aligned with their 3-fold axes almost coincident along c; however, with only one tetrabromoferrate(III) form present, $z = 4$ gives but four tetrahedra per unit cell. No magnetic measurements have been reported for either of these compounds.

Magnetic Properties. Single-crystal magnetic susceptibility measurements carried out parallel to the a and c axes for $[4\text{-Cl(py)H}]_3Fe_2Br_9$ show normal behavior for a three-dimensionally ordering antiferromagnet; c being the easy axis or $\chi_\parallel$ and a the normal $\chi_\perp$. At $T_c = 7.96$ K for data collected along the b axis, a sharp peak is observed in both the real and imaginary components of the complex susceptibility. This is indicative of a canting of the c-aligned spin magnetic moments of the iron ion toward the b axis, giving rise to a net weak ferromagnetic moment in this direction. Canting is known to occur in coordination compounds containing the isoelectronic ion Mn^{2+}. However, the $A_3Fe_2X_9$ series is the first report for an ^6S ground-state Fe(III) complex.

Because crystal field splittings play only a minor role for S-state ions, such as Fe^{3+}, one expects to find these ions among those that produce highly isotropic Heisenberg model type interactions. Two compounds of this isostructural series having stoichiometry $A_3Fe_2X_9$ do give small values for the anisotropy energy and $\alpha \approx 10^{-2}$, a measure of anisotropy, as derived from phase diagram measurements, and serve as good approximations of the sc Heisenberg AF model.[1] Our calculations of appropriate Fe–Fe distances to determine the number of nearest magnetic neighbors are inconclusive in enabling a choice between the sc, bcc, and fcc lattice types, in part due to the variation of Fe···Fe distance along c. A detailed analysis will be given with the structure and superexchange correlations.

Values of the exchange constant, $|J|/k_B$, calculated for both the sc and bcc models, give more consistent results for the sc model, following the theoretical predictions[18] given by $\chi_{max}|J|/N_0g^2\mu_B{}^2$

(17) Hackert, M. L.; Jacobson, R. A. *Acta. Crystallogr.* **1971**, *B27*, 1658.

(18) Puértolas, J. A.; Navarro, R.; Palacio, F.; Bartolomé, J.; Carlin, R. L. *Phys. Rev. B* **1982**, *26*, 395.

Table VI. Superexchange Path Lengths

path	length, Å	path	length, Å	path	length, Å
$[4\text{-Cl(py)H}]_3Fe_2Br_9$		$[4\text{-Br(py)H}]_3Fe_2Cl_{1.3}Br_{7.7}$		$[4\text{-Cl(py)H}]_3Fe_2Cl_9$	
Type II		Type II		Type II	
Fe(1) --- Br(2) (3.90) Br(4) ----- Fe(1)	8.58	Fe(1) --- Br(2) (3.98) Br(4) ----- Fe(1)	8.64	Fe(1) --- Br(2) (4.10) Br(4) ----- Fe(1)	8.45
Fe(1) --- Br(2) (4.33) Br(6) ----- Fe(2)	9.01	Fe(1) --- Br(2) (4.20) Br(6) ----- Fe(2)	8.90	Fe(1) --- Br(2) (4.27) Br(6) ----- Fe(2)	8.63
Fe(1) --- Br(2) (4.08) Br(8) ----- Fe(2)	8.78	Fe(1) --- Br(2) (4.32) Br(8) ----- Fe(2)	9.00	Fe(1) --- Br(2) (4.30) Br(8) ----- Fe(2)	8.66
Fe(1) --- Br(3) (3.91) Br(5) ----- Fe(2)	8.58	Fe(1) --- Br(3) (4.07) Br(5) ----- Fe(2)	8.67	Fe(1) --- Br(3) (4.18) Br(5) ----- Fe(2)	8.54
Fe(1) --- Br(3) (4.56) Br(6) ----- Fe(2)	9.24	Fe(1) --- Br(3) (4.45) Br(6) ----- Fe(2)	9.08	Fe(1) --- Br(3) (4.43) Br(6) ----- Fe(2)	8.80
Fe(1) --- Br(4) (4.01) Br(6) ----- Fe(2)	8.69	Fe(1) --- Br(4) (4.02) Br(6) ----- Fe(2)	8.68	Fe(1) --- Br(4) (4.04) Br(6) ----- Fe(2)	8.40
Fe(1) --- Br(4) (3.83) Br(8) ----- Fe(2)	8.52	Fe(1) --- Br(4) (3.79) Br(8) ----- Fe(2)	8.44	Fe(1) --- Br(4) (3.89) Br(8) ----- Fe(2)	8.25
Fe(2) --- Br(5) (4.15) Br(7) ----- Fe(2)	8.83	Fe(2) --- Br(5) (4.35) Br(7) ----- Fe(2)	8.94	Fe(2) --- Br(5) (4.33) Br(7) ----- Fe(2)	8.70
Type III		Type III		Type III	
Fe(1) (4.44) Br(6) ---- Fe(2)	6.79	Fe(1) (4.28) Br(6) ---- Fe(2)	6.63	Fe(1) (4.42) Br(6) ---- Fe(2)	6.60
Fe(2) (6.14) Br(1) ---- Fe(1)	8.48	Fe(2) (6.08) Br(1) ---- Fe(1)	8.40	Fe(2) (6.00) Br(1) ---- Fe(1)	8.18

= 0.0394 (1), $k_BT(\chi_{max})/|J|S(S+1) = 3.07$ (8) and $k_BT_c/|J|S(S+1) = 2.84$. With $\chi_{max} = 0.1313$ emu mol^{-1}, $T(\chi_{max}) = 8.97$ K, and $T_c = 7.96$ K, the three values of the exchange constant, $|J|/k_B$, obtained for the sc model, 0.45, 0.33, and 0.32 K, are in fair agreement with the 0.47-K value obtained from comparison of the magnetic susceptibility data to HTS expansion and Padé approximant sc Heisenberg 3D spin $^5/_2$ theoretical curves. However, $|J|/k_B$ values calculated from T_c and $T(\chi_{max})$ differ substantially from that obtained from χ_{max}. A small contribution to $\chi_\perp$ from the weak ferromagnetic peak was observed, which increased the uncertainty of $T(\chi_{max})$ and χ_{max}; T_c is known more precisely as the value at the very sharp canting peak temperature.

We reported the phase diagrams in the $H-T$ plane for both $[4\text{-Cl(py)H}]_3Fe_2Cl_9$ and $[4\text{-Br(py)H}]_3Fe_2Cl_9$ in the previous paper.[1] These salts have ordering temperatures, respectively, of 2.73 and 2.34 K. We were unable to measure the phase diagram of the salts reported in this paper, for with substantially higher transition temperatures (a factor of 3), the external fields necessary to define the SF-P boundary, especially near the critical field, are too high and unavailable to us.

Partial substitution of Cl for Br on Fe(III) in the parent compound $[4\text{-Br(py)H}]_3Fe_2Br_9$, enabled by the high lability of high-spin iron(III) centers, complicates the superexchange even further. This is evident from the susceptibility data given in Figure 6. Broadened susceptibility peaks appear, which may actually be several overlapping peaks. Canting only occurs in multisublattice systems. Because the Cl atoms statistically prefer sites X(3) and X(7), as can be seen from the site occupation statistics given in Table IV, species such as $[FeBr_4]^-$, and $[FeBr_3Cl]^-$ may be clustered, forming domains in the crystal, rather than alternating in a regular isotropic pattern. This might cause exchange pathways in different regions to become important at different temperatures, producing multiple overt canting peaks in the susceptibility data.

Structure and Superexchange Correlations. Alignment and small distortions of the tetrahedra seen in Figure 4 allow the three X···X contacts between intramolecular Fe(2) and Fe(1) atoms to have the dissimilar values of 4.33, 4.56, and 4.01 Å. Analogous interactions to the X(1) side of the tetrahedra are absent because the distances X(N)···X(1), where N = 5, 7, and 8, are far longer than all others considered. The overall three-dimensional scheme of Figure 3, with various nonidentical Fe–X···X–Fe superexchange pathways, seems to represent reliably the ordering observed for the compounds $[4\text{-X(py)H}]_3Fe_2X_9$; however, the interactions pictured do not closely resemble those of an ideal sc Heisenberg antiferromagnet nor does the number of nearest neighbors lead to selection of a sc model. In fact, because of the alternating distances between the tetrahedra along c, the actual number of nearest neighbors is one. It might then seem reasonable to consider the superexchange as being between dimers, with three almost equivalent pathways, as depicted in Figure 4, and to include the interdimer interactions in a molecular field correction. This analysis has been applied to previous systems with success.[19] This approach is not applicable here, however, for two reasons. First, it assumes the intradimer interaction to be the strongest interaction, and there is little evidence of broadness in the susceptibility curve, which would indicate the dominance of low-dimensional or short-range order. Second, it is noticed that for the isostructural series of compounds of stoichiometry $[4\text{-X(py)H}]_3Fe_2X_9$, that an increase in T_c among these compounds (along with $|J|/k_B$), coincides with an increase in the c unit cell length. If the primary superexchange paths are along c, then c should decrease and not increase with increasing T_c. No trend is seen for a correspondence of $|J|/k_B$ with ordered unit lengths along a or b, cell volume, V, or values of the angle β.

An examination of the eight closest Br···Br contacts between nearby coordination spheres (type II interactions in Table VI) reveals that only two of these contacts decrease in length with an increase in T_c for these similar compounds. These are the X(5)···X(3) and X(4)···X(2) contacts, which are each roughly in the $a-b$ plane. It is proposed that these interactions may be considered most responsible for the increase in exchange. Another contact in the same plane, X(4)···X(8), is very short for all three compounds, and although its length does not vary as T_c, it is probably important in superexchange. The interaction X(6)···X(4) is almost constant for the three compounds compared in the series and, being also close to the van der Waals interhalide radii, could account for the observed third dimension in ordering.

In the scheme outlined above, Br(1) and Br(7) are least involved in the superexchange scheme, and Br(4) seems most active. Of the two strongest pathways, one includes Br(3), which for the mixed-halide compound is one of the sites statistically preferred by Cl (34% occupancy). The complicated susceptibility curves observed for this compound lend credence to the considerable importance of a path that incorporates a site with statistically mixed occupancy.

(19) Joung, K. O.; O'Connor, C. J.; Sinn, E.; Carlin, R. L. *Inorg. Chem.* **1979**, *18*, 804.

The similarity of magnetic ordering of these compounds to a sc Heisenberg model, then, is due to the overall three-dimensional and fairly isotropic superexchange. That the sc model falls short of an accurate physical description of these compounds is not unexpected, for the model approximates the magnetic ion as having six equivalent and equidistant nearest neighbors and does not consider such potentially important effects as further neighbor and dipole–dipole interactions. These factors, as well as the effects of additional small changes in the composition of the $A_3Fe_2X_9$ salts on structural magnetic properties including specific heat measurements and neutron spin structures, will be considered in the future, in an effort toward a better understanding of some of the fundamentals of magnetomolecular architecture.

Acknowledgment. We thank Dr. K. R. Seddon and Dr. Jalal Zora for introducing us to this series of compounds. We also thank Ramon Burriel for helpful suggestions for this manuscript. This work was supported by the Solid State Chemistry Program of the Division of Materials Research of the National Science Foundation, under Grants DMR-8515224 and DMR-8815798. Acknowledgment is made to the donors of the Petroleum Research Fund, administered by the American Chemical Society, for partial support of this research. Work at Argonne National Laboratory was sponsored by the U.S. Department of Energy, Office of Basic Energy Sciences, Division of Materials Sciences, under Contract W-31-109-Eng-38.

Supplementary Material Available: Tables of crystallographic parameters (Table S1), anisotropic thermal parameters (Tables S2 and S5), and distances and angles (Tables S3 and S6) (8 pages); tables of structure factors (Tables S4 and S7) (38 pages). Ordering information is given on any current masthead page.

Contribution from the Laboratoire de Chimie de Coordination du CNRS,† 205 route de Narbonne, 31077 Toulouse Cedex, France, and Department of Chemistry, University of Poona, Poona, 411007 India

Iron(II) Complexes of Ortho-Functionalized *p*-Naphthoquinones. 2. Crystal and Molecular Structure of Bis(aquo)bis(lawsonato)iron(II) and Intermolecular Magnetic Exchange Interactions in Bis(3-aminolawsonato)iron(II)

Prafulla Garge,[1a] Rajeev Chikate,[1a] Subhash Padhye,*[,1a] Jean-Michel Savariault,[1b] Philippe de Loth,[1b] and Jean-Pierre Tuchagues*[,1b]

Received July 11, 1989

Two related complexes [Fe(lawsonato)$_2$(H_2O)$_2$] (**1**) and [Fe(3-aminolawsonato)$_2$(CH_3OH)] (**2**), wherein lawsonato is the anion of 2-hydroxy-1,4-naphthoquinone, have been synthesized and studied. **1** crystallizes in the monoclinic system, space group $P2_1/c$ with $Z = 2$, $a = 5.036$ (3) Å, $b = 16.448$ (3) Å, $c = 10.710$ (3) Å, and $\beta = 99.75$ (4)°. The structure was solved by the heavy-atom method and refined to conventional agreement indices $R = 0.051$ and $R_w = 0.057$ with 1444 unique reflections for which $I > 2\sigma$. The three-dimensional network of the crystal results from the linking of infinite chains of [Fe(lawsonato)$_2$(H_2O)$_2$] molecules through hydrogen bonds. These chains consist of complex molecules doubly hydrogen-bonded along the [100] direction. Each complex molecule comprises two bidentate lawsone ligands coordinated to the ferrous iron center in their fully oxidized *p*-quinone form and two trans water molecules. The resulting coordination sphere can be described as a rhombically distorted octahedron. The synthesis, IR, UV–visible, and Mössbauer spectra, and thermogravimetric, variable-temperature magnetic susceptibility, and cyclic voltammetry studies of **2** are described. Both 3-aminolawsone ligands are in their fully oxidized form, and the coordinating centers are the C(2) phenolate oxygen and C(3) amino nitrogen atoms. Variable-temperature magnetic susceptibility studies establish the presence of isotropic magnetic exchange interactions between the high-spin iron(II) centers of a dimeric species ($J = -1.6$ cm^{-1}) and crystalline field anisotropy of the ferrous ion ($D = 4.9$ cm^{-1}). The dimeric structural arrangement of **2** implies a N_2O_4 ligand environment holding two *p*-naphthoquinone moieties at ca. 4 Å from the ferrous center and can therefore serve as a basis for studying the effect of quinone oxidation state changes on electronic and magnetic properties of the iron(II)–quinone couple in the "ferroquinone complex" of photosynthetic bacteria and photosystem 2.

Introduction

Quinones play an integral role in many biological electron-transfer processes, particularly respiration and photosynthesis.[2] Some of these reactions are catalyzed by metal ions like copper, iron, manganese, and molybdenum, although mechanistic aspects of these interactions have not been fully elucidated.[3] During these processes, quinones are reversibly reduced to either semiquinone radical anions or dianionic catechols with concomitant oxidation of the divalent metal ions.

Studies on ubiquinones have shown that they function as electron shuttles between various flavoprotein dehydrogenases in the electron-transport chain.[4] Similarly, plastoquinones and catechols are known to be involved in green plants and enzymatically catalyzed reactions of oxygen.[5] In view of the roles of quinones in electron-transport chains, it is important to characterize and thoroughly study metal complexes with quinone derivatives of biological relevance. For this purpose, hydroxyquinone ligands of natural occurrence have been studied for some time.[6] More recently, we have reported on the mononuclear iron(II) complexes of ortho-functionalized *p*-naphthoquinones, showing that the bound quinone ligands are in their fully oxidized form.[7]

In the present paper, the molecular crystal structure of one such high-spin ferrous complex of lawsone is described for the first time. Lawsone is the 2-hydroxy-1,4-naphthoquinone pigment found in

† Unité No. 8241 liée par conventions à l'Université Paul Sabatier et à l'Institut National Polytechnique de Toulouse.

(1) (a) University of Poona. (b) Laboratoire de Chimie de Coordination du CNRS.
(2) (a) Thomson, R. H. *Naturally Occurring Quinones*; Academic Press: New York, 1971. (b) Morton, R. A. *Biochemistry of Quinones*; Academic Press: New York, 1965.
(3) Buchanan, R. M.; Pierpont, C. G. *Coord. Chem. Rev.* **1981**, *38*, 45–87.
(4) (a) Orme-Johnson, N. R.; Orme-Johnson, W. H.; Hansen, R. E.; Beinert, H.; Hatefi, Y. *Biochem. Biophys. Res. Commun.* **1971**, *44*, 446–452. (b) Tikhonov, A. N.; Burvaev, D. S.; Grigolva, I. V.; Konstantinov, A. A.; Kzenzenko, M. Y.; Ruug, E. *Biofizika* **1977**, *22*, 734–736. (c) Ruzicka, F. J.; Beinert, H.; Schepler, K. L.; Dunham, W. R.; Sands, R. H. *Proc. Natl. Acad. Sci. U.S.A.* **1975**, *72*, 2886–2890. (d) Konstantinov, A. A.; Ruug, E. *Bioorg. Khym.* **1977**, *3*, 787–799.
(5) (a) Feher, G.; Isaacson, R. A.; McElroy, J. D.; Ackerson, I. E.; Okamura, M. Y. *Biochim. Biophys. Acta* **1974**, *368*, 135–139. (b) Wraight, C. A. *FEBS Lett.* **1978**, *93*, 283–287. (c) Govindjee, Ed. *Bioenergetics of Photosynthesis*; Academic Press: New York, 1974.
(6) (a) Padhye, S. B.; Kulkarni, B. A. *J. Phys. Chem.* **1975**, *79*, 927–928. (b) Padhye, S. B.; Kulkarni, B. A. *J. Magn. Res.* **1974**, *16*, 150–152.
(7) (a) Padhye, S.; Garge, P.; Gupta, M. P. *Inorg. Chim. Acta* **1988**, *152*, 37–42. (b) Garge, P.; Padhye, S.; Tuchagues, J. P. *Inorg. Chim. Acta* **1989**, *157*, 239–249.

0020-1669/90/1329-3315$02.50/0